Review

Brian J. Kirby[1]
Ernest F. Hasselbrink Jr.[2]

[1]Microfluidics Department, Sandia National Laboratories, Livermore, CA, USA
[2]Mechanical Engineering Department, University of Michigan, Ann Arbor, MI, USA

Zeta potential of microfluidic substrates: 1. Theory, experimental techniques, and effects on separations

This paper summarizes theory, experimental techniques, and the reported data pertaining to the zeta potential of silica and silicon with attention to use as microfluidic substrate materials, particularly for microchip chemical separations. Dependence on cation concentration, buffer and cation type, pH, cation valency, and temperature are discussed. The Debye-Hückel limit, which is often correctly treated as a good approximation for describing the ion concentration in the double layer, can lead to serious errors if it is extended to predict the dependence of zeta potential on the counterion concentration. For indifferent univalent electrolytes (*e.g.*, sodium and potassium), two simple scalings for the dependence of zeta potential on counterion concentration can be derived in high- and low-ζ limits of the nonlinear Poisson-Boltzman equation solution in the double layer. It is shown that for most situations relevant to microchip separations, the high-ζ limit is most applicable, leading to the conclusion that the zeta potential on silica substrates is approximately proportional to the logarithm of the molar counterion concentration. The ζ *vs.* pH dependence measurements from several experiments are compared by normalizing the ζ based on concentration.

Keywords: Microfluidic substrates / Miniaturization / Review / Zeta potential
DOI 10.1002/elps.200305754

Contents

Correspondence: Brian J. Kirby, PhD, Microfluidics Department, Sandia National Laboratories, P.O. Box 969, Livermore, CA 94551, USA
E-mail: bjkirby@sandia.gov
Fax: +925-294-3020

Abbreviations: EDL, electrical double layer; **GCS**, Gouy-Chapman-Stern; **OHP**, outer Helmholtz plane

1 Introduction

Understanding and managing electroosmotic flow is central both to microchip separations and to the manifold techniques associated with separations analysis (sample injection, sample concentration, *etc.*). Microchip separations typically employ electric fields, owing both to the importance of a number of well-established electrokinetic separation techniques (electrophoresis, isoelectric focusing, micellar electrokinetic chromatography, gel electrophoresis, and electrochromatography) and to the relative ease of integration of voltage sources and electroosmotic manipulation of fluids. The zeta potential, or potential at the solid-liquid interface (more precise definitions are to follow), is a fundamental parameter in models of electrical double layers and their associated properties (electrode capacitance, electroosmosis, *etc.*). The potential applied

to an electrode is inherently well-defined and easily measured, hence the zeta potential is a natural parameter to use to describe electrochemical properties such as electrode capacitance. However, when the same double layer equations are extended for application to electroosmosis, interpretation of the zeta potential becomes much more complicated, since the zeta potential, rather than being straightforwardly controlled by an input voltage, is a result of detailed chemistry and ion distributions at the diffuse interface between substrate and solution. This chemical dependence, combined with the strictly inferential nature of zeta potential measurements, makes it much more difficult to measure and interpret the zeta potential for modeling of electroosmosis. Invariably, zeta potential measurements made in different laboratories do not agree as well as could be hoped.

The purpose of this paper and its companion [1] is to summarize the wide variety of reported data on the zeta potential of microfluidic substrate materials, searching in particular for commonality, reductive scaling relations, and engineering predictive capability. In so doing, we hope also to highlight areas in which focused research will lead to improved understanding and better system design. In particular, focus will be placed in this paper on scaling relations that allow meaningful comparisons between experiments with widely varying parameters. The paper is organized as follows: first, double layer theory is presented specifically as it relates to electroosmotically driven double layers. This highlights the separability of the pH-dependence of ζ (attributable primarily to protonation and adsorption at the wall) and the concentration dependence of ζ (for indifferent counterions, attributable primarily to electrical shielding by the overconcentration of counterions in the diffuse layer). Furthermore, this shows how the results of zeta potential measurements depend directly on the model used to infer ζ. Second, techniques for measuring zeta potential are discussed, with specific attention to rigorous interpretation of published data and pitfalls in experimental techniques. Third, observed zeta potential results on silica and silicon substrates are summarized in the context of the presented theory. Finally, the impact of these results on electrophoretic separations is addressed. In the companion to this paper [1], polymer substrates will be discussed in a similar fashion.

2 Theory of zeta potential and electroosmosis

In this section, a cursory introduction to electrical double layer theory is presented with specific attention to both the zeta potential and the resulting electroosmotic flow observed in an electric field. The net charge density on a microfluidic substrate in contact with an aqueous solution gives rise to an electrical double layer and, in the presence of an electrical field, electroosmosis. In general, protonation, deprotonation, adsorption and other reaction equilibria define a net charge density, q'' (units charge per unit area, *e.g.*, C/cm^2), on the surface. This charge density creates an electric field, drawing oppositely charged ions (counterions) towards it and driving like-charged ions (co-ions) away (Fig. 1). For example, for an aqueous KCl solution in contact with silica at pH 7, the H^+ (H_3O^+) and K^+ ions preferentially concentrate near the negatively charged surface. This shielding layer is commonly known as a Debye layer or electrical double layer (EDL). Details of the structure of the EDL have historically been of significance to both electrochemistry as well as colloid science, and in-depth reviews on double layer structure can be found in several texts and handbooks [2–7].

Most double layer models are variations of the Gouy-Chapman-Stern (GCS) model [2], wherein the EDL is comprised of a diffuse layer and a Stern layer. The diffuse layer gives rise to electroosmosis and is the region of the EDL most pertinent to calculations of electroosmosis in microchip separation devices. The Stern layer of counterions

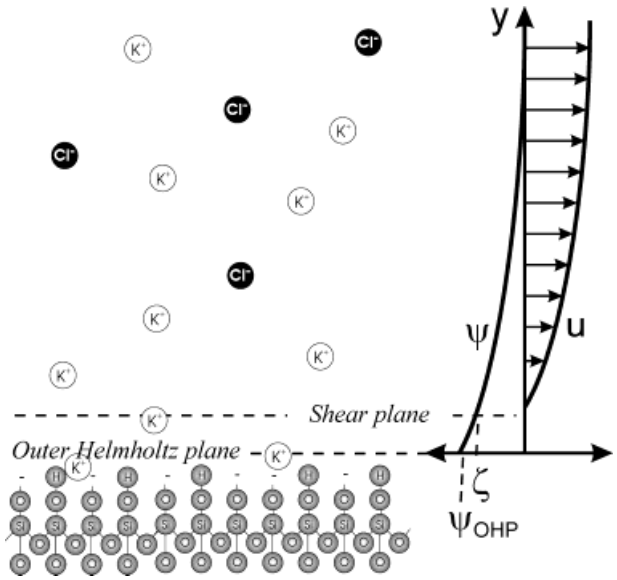

Figure 1. Conceptual representation of the electrical double layer at the interface of silica and a weak KCl solution. ψ, local potential; OHP, outer Helmholtz plane; *u*, local electroosmotic velocity. Negative surface charge stems from deprotonated silanols. Shielding of this surface charge occurs due to adsorbed ions inside the OHP and by mobile ions in a diffuse layer. Potential and EOF velocity profiles are shown at right. The shear plane is where hydrodynamic motion becomes possible; ζ is the potential at this plane. Illustration not to scale.

lies at the distance of closest approach from the surface, dictated by the size of the ion. The existence of the Stern layer helps to describe both the dependence of electrode capacitance on counterion size and the functional form of electrode capacitance at high counterion concentration. Counterions in the Stern plane do not move normal to the surface, but measurements of so-called anomalous conductivity suggest that the ions may still move laterally in certain situations [8–17]. The outer edge of the Stern layer is called the outer Helmholtz plane (OHP); the distance from the wall is denoted y_{OHP} and the potential is denoted ψ_{OHP}. More complex models are necessary to explain behavior resulting from complex surface molecular structures at certain interfaces as well as to predict ζ quantitatively [18–20]. Employing molecular dynamics simulations to gain insight into the behavior of molecules in the first nanometer or so near a surface is also an active area of research [16, 21, 22].

The potential, ion concentration, and velocity profiles in the diffuse portion of the EDL lead directly to electroosmosis and are the pertinent parameters for the purposes of separations in various substrates. These are found by combining the Poisson equation for an electric charge density ρ_e and electric field $\nabla\psi$ in a medium of permittivity ε, with the assumption of Boltzmann equilibrium in the charge distribution, leading to

$$\nabla^2\psi = \frac{-\rho_e}{\varepsilon} = -\frac{1}{\varepsilon}\sum_i n_{o,i}\, ez_i \exp\left(-\frac{ez_i}{kT}\psi\right) \qquad (1)$$

where the summation is over all ionic species *i*, and $n_{o,i}$ refers to the concentration at a reference potential, which is taken at $\psi = 0$ for convenience. *e* is the elementary charge, z_i is the valency of each ionic species, *k* is the Boltzmann constant, and *T* is the temperature. This is a nonlinear partial differential equation for ψ as a function of space that can be solved analytically only for a few special cases. For a symmetric electrolyte ($z^+ = |z^-| = z$; *e.g.*, KCl) the right hand side becomes $(2n_o ez/\varepsilon)\cdot\sinh(ez\psi/kT)$.

The boundary conditions on Eq. (1) are a matter of current research. An active area of research in interface science is the distance from the wall at which the no-slip boundary condition for fluid flow should be applied, and this depends on the properties of the interface [23, 24]. Some models define a shear plane at a distance y_s where the potential is termed the zeta potential (ζ), as shown in Fig. 1; defining *y* as the distance from the shear plane, the boundary conditions become $\psi(y = 0) = \zeta$, and $\psi(y \to \infty) \to 0$. Many subtle ramifications of the possibility that $\zeta \neq \psi_{OHP}$ have been reviewed elsewhere [4, 9]. Because of the variations in the application of boundary conditions for Eq. (1), electrokinetic data obtained in different ways may lead to different inferred values of ζ. The remainder of this discussion is applied only to idealized surfaces, and so the exact solution of this fully nonlinear equation (for symmetric binary electrolytes) is [2]:

$$\psi^* = 2\ln\left[\frac{1+\tanh(\zeta^*/4)\exp(-y/\lambda_D)}{1-\tanh(\zeta^*/4)\exp(-y/\lambda_D)}\right] \qquad (2)$$

where normalized variables $\psi^* = \psi ze/kT$, $\zeta^* = \zeta ze/kT$ are defined for brevity. For $z = 1$ and at 298K, $\zeta^* \cong \zeta/25$ mV. The length scale $\lambda_D = (\varepsilon kT/2n_o e^2 z^2)^{1/2}$ is commonly known as the Debye length, where n_o is the bulk electrolyte number density. A useful rule of thumb is that for a symmetric electrolyte in water at 298K, λ_D [nm] $\cong 9.6/c^{1/2}z$, where *c* is the electrolyte concentration in mM. Profiles of this potential distribution are shown in Fig. 2.

To our knowledge, the fully nonlinear form of the Poisson-Boltzmann equation has been solved only for the region above an infinite flat plate in an infinite fluid for symmetric electrolytes ($z^+ = |z^-| = z$). Semianalytical solutions between infinite parallel plates have been provided, requiring numerical evaluation of elliptic integrals [25]. No analytical solutions are available for the etched cross-section geometries encountered in microchips. However, solutions are possible in the Debye-Hückel limit, in which it is assumed that $z\psi$ is not large compared to kT/e (about

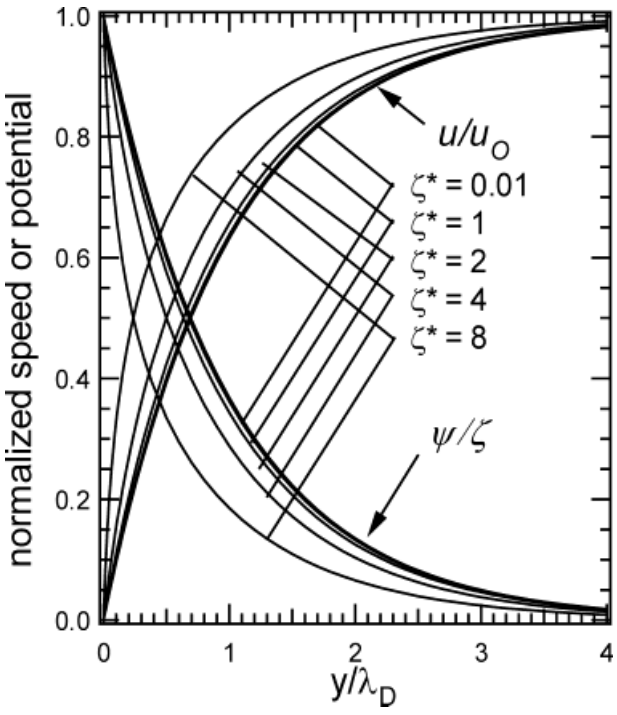

Figure 2. Calculated potential distribution from Eq. (2). Similar plots for tubes and channels are available in [25–27]. *u*, electroosmotic speed; u_0, value at infinity; ψ, potential; ζ, potential at shear plane; ζ^*, normalized ζ.

25 mV at 25°C) everywhere in the fluid. With this assumption, the equation can be linearized by approximating $\sinh(\psi^*) \cong \psi^*$ for small ψ^*. For an infinite flat plate with nothing but a symmetric electrolyte above it, the Debye-Hückel solution for the potential is a simple exponential decay: $\psi = \zeta\exp(-y/\lambda_D)$. Profiles of ψ/ζ near a flat plate are shown in Fig. 2; the Debye-Hückel solution is within 10.7% of the exact solution at all y as long as $\zeta < 100$ mV (at 25°C), but at higher ζ the shielding layer is actually thinner than λ_D. The Debye-Hückel solution between two parallel plates (approximated by a very wide, shallow microchannel) is $\psi = \zeta\ \cosh(y/\lambda_D)/\cosh(h/\lambda_D)$, where h is the half-width and y is taken from the center of the channel; in a round capillary the Debye-Hückel solution is $\psi = \zeta\, I_o(r/\lambda_D)/I_o(a/\lambda_D)$, where I_1 and I_0 are modified Bessel functions of the first kind, r is the radial distance from the central axis, and a is the capillary radius [26]. The Debye-Hückel solution is useful for approximating the ion distribution in the double layer; however, as will be seen later, it can fail badly if erroneously extended to predict the dependence of zeta potential at low counterion concentrations.

For microchip separation devices, the most important consequence of the EDL is electroosmosis in microchip channels. An electric field introduced down the length of an electrolyte-filled capillary or microchannel induces the net charge in the EDL to migrate, carrying the rest of the fluid in the capillary with it by the action of viscosity. The governing equation for this flow is a simplified form of the Navier-Stokes equations in which the flow is presumed steady and the nonlinear advective term is assumed negligible:

$$\nabla\mathbf{P} = \eta\nabla^2\mathbf{u} + \rho_e\mathbf{E} \tag{3}$$

Here, **P** is the pressure, η is the dynamic viscosity, and **u** and **E** are the velocity and electric field vectors, respectively. The nonlinear advective term from the Navier-Stokes equations can be ignored since, in virtually all electroosmotic flows, inertial forces are negligibly small compared to pressure and viscosity forces; *i.e.*, the Reynolds number, $\rho Ud/\eta$, is much less than unity (ρ is the fluid mass density; U is the mean fluid speed; d is a length scale characterizing the velocity gradients, *e.g.*, microchannel diameter). In the absence of a pressure gradient, the left hand side is zero; substituting in from Poisson's equation ($\varepsilon\nabla^2\psi = -\rho_e$) gives

$$\nabla^2\mathbf{u} = (\varepsilon\mathbf{E}/\eta)\nabla^2\psi \tag{4}$$

For any unidirectional flow with uniform electrical field, (*e.g.*, flat plate, capillary or parallel flat plate), this problem can be solved by mapping $u(\psi)$ rather than $u(y)$. In the infinite plate problem shown above, using the same boundary conditions on ψ, the boundary condition $u(y = 0) = 0$ and $u(y \to \infty) \to U$ become $u(\psi = \zeta) = 0$ and $u(\psi \to 0) \to U$, and so we can write in general (without Debye-Hückel linearization) that

$$u = -\frac{\varepsilon\zeta}{\eta}E\left(1 - \frac{\psi}{\zeta}\right) \tag{5}$$

The solution for $\psi(y)$ (either in the Debye-Hückel limit or fully nonlinear solution) can be substituted to get the velocity profile $u(y)$. Similarly, concentrations of the counterions and co-ions in the solution may be obtained directly from Boltzmann equilibrium (Eq. 1). Since $\psi \to 0$ far from the wall, the velocity approaches $U = -(\varepsilon\zeta/\eta)E$; the factor $-\varepsilon\zeta/\eta$ is therefore known as the electroosmotic mobility, μ_{eo}.

Since the EDL is normally only a few nanometers thick, the velocity profile in uniform microchannels or capillaries is essentially uniform, except for the boundary region within the EDL. In channels where λ_D is much smaller than the channel diameter (and curvature), the double layers do not overlap, and the velocity profile in the EDL is very close to the velocity profiles $u^* = u/\mu_{eo}E$ above a single infinite plate as shown in Fig. 2. An important point to note from Eq. (5) is that finite EDL thickness ensures that the apparent μ_{eo} inferred from measuring the speed of an analyte band will always be lower than the actual μ_{eo}, although the error becomes negligible if $\lambda^* < 0.01$; [27, 28] give analytical expressions and show plots of the discrepancy expected. A similar issue exists for small spherical particles in solution; for the case of very small particles, the apparent electrophoretic mobility of the particles falls from $\varepsilon\zeta/\eta$ to $(2/3)\varepsilon\zeta/\eta$ due to the finite EDL thickness [29], so great care must be taken when interpreting electrokinetic data from particles.

Since different separation techniques employ varying buffer concentrations, the effects of ionic strength and electrolyte valency on zeta potential must be predicted. The effect of counterion concentration arises from at least two effects: (i) The counterion may be adsorbed to the surface, or into the Stern layer, and thereby change the net surface charge density that must be shielded by the diffuse region. Most predictive models for ζ therefore include equilibrium constants for H^+/metal-ion substitution reactions and binding activities. Boltzmann partitioning leads to a zeta potential that varies linearly with the logarithm of the counterion concentration. (ii) Changing the thickness of the EDL changes the ζ-potential directly, even for a fixed surface charge density. This follows by setting the total charge in the diffuse layer opposite in sign and equal in magnitude to the surface charge,

$$q'' = -\int_0^\infty \rho_e dy = -\varepsilon \left.\frac{\partial \psi}{\partial y}\right|_{wall} \quad (6)$$

where the term on the far right-hand side, (the slopes are evaluated at the wall), is derived by direct substitution of the Poisson equation (1). Substitution of the Debye-Hückel solution leads to $\zeta = \lambda_D q''/\varepsilon$, while substitution of the fully nonlinear solution gives

$$\sinh(-e\zeta/2kT) = q''\lambda_D e/2\varepsilon kT \quad (7)$$

If the surface charge density is unaffected by counterion strength, and all the shielding is performed by the diffuse portion of the double layer, then the dependence of ζ on counterion concentration (given constant temperature, dielectric constant) can be shown to be

$$\zeta \sim \lambda_D \sim c^{-1/2} z^{-1} \quad \text{when } \zeta \ll 2kT/e \quad (8)$$

$$\zeta \sim \log \lambda_D \sim a_0 + a_1 \log (cz^2) \quad \text{when } \zeta \gg 2kT/e \quad (9)$$

for a symmetric electrolyte. Equations (8) and (9) follow, respectively, from the small- and large-x limits of sinh(x), that is, sinh(x) → x or sinh(x) → exp(x)/2.

The applicability of the simplified relations in Eqs. (8) and (9) must be carefully examined in light of the extensive use of both scalings in the literature. The low-ζ scaling ($\zeta \sim 1/c^{1/2}$) has been more commonly discussed in the separations literature [30–36], while the high-ζ scaling ($\zeta \sim$ log c) has been more commonly used in the interface science literature [20, 37]. Equation (8) gives the counterion concentration dependence of the zeta potential at low zeta potential, and is generally applicable for silica at low pH (<3.5) or high counterion concentration (>200 mM). Its range of applicability is limited, and it completely fails to describe zeta potential variation at low concentration. For example, if Eq. (8) is used to extrapolate ζ from the 100 mM value ($\zeta \approx 20$ mV at pH = 6, 20°C) to 1 mM and 0.01 mM, the resulting values are 200 mV and 2000 mV, respectively – both of these are incorrect and the latter is in error by more than a factor of 10. Many references in the separations literature discuss Eq. (8) without specifying in detail the assumptions and limitations attendant with its use, and often Eq. (8) is applied well outside its range of validity. Further, *ad hoc* adjustments to Eq. (8) have been applied; these adjustments can be misleading since they purport to support the scaling in Eq. (8) but on closer examination are phenomenological approximations of Eq. (9). For example, [33, 36] both fit lines to plots of migration time *versus* $c^{1/2}$ or electroosmotic mobility *versus* $c^{-1/2}$, and claim that the linear fits imply that scaling similar to Eq. (8) applies. However, these linear fits occur over too narrow a domain of c to be conclusive, and in fact these plots do not intercept the origin, as Eq. (8) suggests they should. Replotting the data from [33], as ζ *vs.* $-\log c$ ($-\log c$ = pC, where c is in M), yields data that fall on a line with intercept that is consistent with most silica investigations (this can be seen later, in Fig. 3). It has been suggested to modify the $\zeta \sim 1/c^{1/2}$ scaling by postulating cation adsorption equilibria combined with a Stern layer thickness determined from fits to data [32, 34]. However, it was found that this combined scaling/modeling approach can fit the data only through Stern layer thicknesses that vary with experimental conditions and are on the order of 100 nm, which are inconsistent with other physical descriptions of the Stern layer.

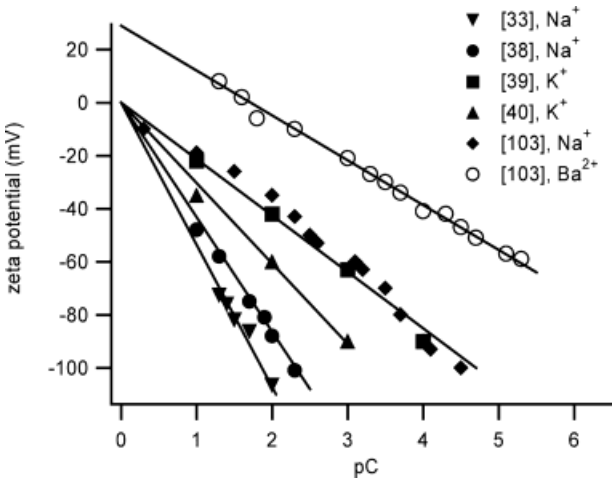

Figure 3. Zeta potential of silica in contact with aqueous solutions plotted *versus* the negative logarithm of the counterion concentration (pC). Conditions: [39] pH 5.8, 25°C; [40] pH 7, 30°C; [38] pH 7.85, 35°C; [103] pH 7, 25°C; [33] pH 7, 25°C.

On the other hand, Eq. (9) gives the counterion concentration dependence of the large-magnitude zeta potential, and is generally applicable for silica below 100 mM at pH > 6 and below 10 mM at pH > 3.5. It fails completely to describe zeta potential variation at concentrations above 1 M (in the absence of specific adsorption, the wall charge does not change sign). From a pragmatic standpoint, Eq. (9) leads to a much more satisfactory match with experimental results when generally applied. Reasons for this include: (i) it is valid over a much wider range of concentration; (ii) its absolute deviations are small because it deviates where ζ is small anyway; (iii) for high pH, the concentrations at which it fails badly coincide with concentrations where the Gouy-Chapman double layer theory becomes invalid anyway; and (iv) it is inaccurate at points where the experimental data is very noisy and uncertain, particularly near the substrate's isoelectric point (pI).

This analysis assumes that ions do not show specific adsorption. The logarithmic scaling (Eq. 9) matches well with observations for sodium and potassium buffers on

silica [37–40] but cannot be expected to correctly fit the data for ions that do specifically adsorb (*e.g.*, Ba^{2+} [37]) without addition of a constant term. Melanson [41] argues that the degree to which cations can be expected to adsorb to silica surfaces can be qualitatively inferred from retention times in ion-exchange chromatography, leading to the conclusion that binding affinities can be ordered as [41]

$$M^{2+} >>> M^{+} \tag{10}$$

$$C_a^{2+} > B_a^{2+} > Sr^{2+} \tag{11}$$

$$Cs^{+} \approx Rb^{+} > K^{+} > NH_4^{+} > (C_2H_5)_4N^{+} > (C_4H_9)_4N^{+} > (CH_2OH)_3\,CN^{+} > Na^{+} > Li^{+} \tag{12}$$

and the accuracy of assuming that specific adsorption can be ignored is much better for Li^+, Na^+, and K^+ than it is for Ca^{2+}, Ba^{2+}, and Sr^{2+}. M in Eq. (10) is used to denote a general metal cation, and indicates that divalent cations are much better ion exchange partners than monovalent cations, further that the difference between divalent and monovalent cations is much greater than differences within those groups. For molecules that specifically adsorb, such as many divalent cations, the zeta potential still changes linearly with the log of the concentration over a wide concentration range, but approaches a nonzero value at log c = 0 (Fig. 3). In some cases, similar performance is seen for cationic surfactants [37, 42–44]*.

By assuming ideal surfaces, the treatment above ignores the effect of nanoscale surface roughness on the observed electroosmotic flow. Microfluidic substrates differ from capillaries in that their surface roughness is typically much higher; this roughness leads to geometry-induced changes in the zeta potential and can affect electroosmotic flow. Nonetheless, in the following sections we will show that Eq. (9) at least partially accounts for the observed dependence of zeta potential on electrolyte concentration and valency for many materials. This is useful for engineering extrapolation of existing data, as well as providing a useful framework through which experiments at varying counterion concentrations may be compared.

One other consequence of the EDL is surface conductivity, which is the observed increase in apparent conductivity over the bulk conductivity, due to the double layer and its higher net ion concentrations [16, 45], as can be calculated from ion densities obtained from Eq. (1). The conductivity of the fluid at the shear plane is greater than the bulk conductivity by a factor $\cosh(\zeta e/kT)$, which becomes quite large for $\zeta > 50$ mV. This effect can become noticeable in microchannels of a few microns depth or smaller at modest ionic strengths (~1 mM), and can be a significant source of dispersion when channels of different depths are placed in series, as will be discussed in Section 5.

* Variation of zeta potential with surfactants is a complicated topic, which cannot be covered suitably here. A number of reviews [30, 41] are available for this area.

3 Techniques for measuring zeta potential

In general, zeta potential is measured indirectly using one of three means: (i) by measuring electroosmotic mobility, (ii) by measuring streaming current or streaming potential generated by pressure-driven flow through a conduit, or (iii) by measuring response of a small spherical particle in an applied *E*-field. While the third method is common in studies of colloidal suspensions, this paper is primarily focused on the effects in a channel or other conduit and the work summarized here is restricted to the first two methods. Interpretation of data for submicron particles is more complicated than for capillaries or microchannels larger than 5 μm due to the relative size of the EDL compared to the particle radius [2, 4]; this method has been discussed in detail [46], owing to the importance of colloidal suspensions in a variety of practical industrial, chemical, and pharmaceutical products.

3.1 Electroosmotic mobility

Measuring electroosmotic mobility is a straightforward way to measure the zeta potential. The transit time of an electrically neutral, optically active or conductive tracer through a microchannel or capillary is measured as a function of electrical field, and the electroosmotic mobility is directly related to the zeta potential *via* Eq. (5) assuming thin Debye layers. One convenient method employed in numerous studies is the "current monitoring" method wherein the motion of the fluid is traced by tracking the change in channel conductance as the buffer in the channel is exchanged through electroosmosis [47]. The observed ζ is approximately equal to the average ζ between the two buffers. For accuracy, this technique requires that the smallest concentration difference possible be used, so that the changes in buffer lead to negligible changes in zeta potential and local field strength, which would induce electrokinetically generated pressure gradients [48]. It has been argued [47] that the method can still be reasonably accurate if less than 5% differences in ionic strength are used. A second method involves using an optically detected absorbing tracer that is net-neutral at the electrolyte pH. In all cases, buffered solutions are necessary to stabilize the pH against CO_2 dissolution and other sources of pH drift. A small injection of tracer (as would be performed in CE) is also

preferred over tracking a front, because of the greater ease in determining the center of the peak in the presence of dye impurities. A recent improvement is using a caged- or bleached-dye imaging method [49–52]. The benefit of this method is that the experimentalist can observe the velocity profile, and since all of the spurious effects listed above result in the generation of a pressure-driven flow, they are immediately noticed by the presence of a parabolic velocity profile.

Several sources can contribute error to electroosmotic mobility measurements. Joule heating must be avoided due to the attendant variations in zeta potential and viscosity. The best experimental approach is to measure electroosmotic mobility as a function of electric field and extrapolate to find the zero-field limit. Another potential source of error is pressure-driven flow due to hydrodynamic head differences or surface tension from inlet-to-outlet. The pressure induced by only modest interface curvatures (*e.g.*, 2 mm diameter) can lead to pressure-driven flow speed on the order of 100 μm/s, which can lead to appreciable errors.

In addition to the aforementioned error sources, methods based on measuring electroosmotic flowrate have two potential difficulties: (i) the approximation $u = \varepsilon\zeta E/\eta$ requires that the double layers are quite small ($\lambda^* < 0.01$ or so); corrections based on analytical models [27] are needed for submicron channels. (ii) Hydrolysis or other electrolytic reactions have the equivalent effect of increasing $[H^+]$ at the anode and $[OH^-]$ at the cathode, so the pH and/or conductivity may be altered significantly during the course of an experiment. Significant errors can occur due to the evolution of pH in the reservoirs [53]. These concerns are eliminated by the use of an Ag/AgCl or similar (nonhydrolytic) electrode, or to use very large reservoir capacity for the amount of current drawn. All of these techniques require that the tracer does not affect ζ, which can be difficult to achieve in many polymer microchannels [51].

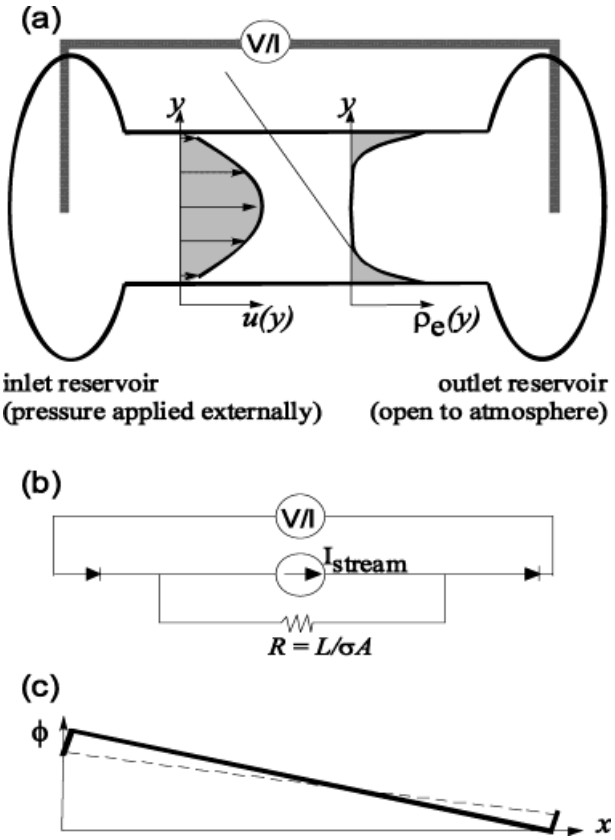

Figure 4. (a) Experimental schematic for streaming current/potential measurements (not to scale). Electrodes through which voltage or current are measured are inserted into reservoirs at either end of a pressurized capillary. Velocity and charge density profiles are shown under the assumption of fully developed laminar flow. (b) Electrical circuit representation of the system. Overpotentials required to transfer electrons at the electrodes are represented by diodes; much more complicated circuit representations (including capacitance) are also possible. (c) Actual (solid line) and apparent (dash line) potential distribution along the capillary during streaming current measurements, due to electrode overpotentials.

3.2 Streaming current/streaming potential

Streaming current and potential techniques measure electrical perturbations brought about when pressure-driven flow in a microchannel carries double layer ions (Fig. 4a). Since the Debye layer has a net charge density, the flux generates a net current known as streaming current. This phenomenon serves as one basis for measuring the electroosmotic mobility of a fluid in contact with a simple planar surface. The current induced by the flow profile $u(y)$ is

$$I_{\text{stream}} = \int_A \rho_e \vec{\mathbf{u}} \cdot d\mathbf{A} \tag{13}$$

where the integral is taken over A, the cross-sectional area of the capillary or microchannel. In general, one must solve the Poisson-Boltzmann equation to get ρ_e, and the Stokes equations to get $\vec{\mathbf{u}}$, for each individual geometry (*e.g.*, as done in [25]). In the limit of Debye-Hückel linearization (low $e\zeta/kT$) and Debye layers that are thin compared to channel diameter or height, a simplified approximation is possible. To derive this, one equates the shear forces at the wall with the pressure difference (ΔP) imposed:

$$\Delta P \cdot A = L \int_S \eta \left.\frac{\partial u}{\partial s}\right|_S ds \tag{14}$$

where *s* is a unit vector normal to the wetted surface area per unit length *S*, and *L* is the length of the conduit. Under the assumption that the Debye layer is thin, the velocity profile can be considered linear close to the wall; comparing the average shear rate at the wall to the imposed pressure leads to

$$I_{\text{stream}} \cong \frac{\varepsilon\zeta}{\eta}\frac{\Delta P}{L}A \tag{15}$$

This applies for any geometry channel, as long as the flow is laminar and fully developed for most of the length (length $>>>$ channel height). Significant corrections are necessary (*e.g.*, as in [25]) if these conditions are not met. The zeta potential, in principle, can be calculated if the current, pressure, channel length, and channel cross-section area are measured and tabulated values of permittivity and viscosity are used. In practice, the slope of the current *vs.* pressure line is measured as the pressure is slowly varied, and ζ is calculated from this slope.

Several potential sources of error can affect streaming current measurements. The first is that Eq. (15) is only an approximation in the thin EDL and Debye-Hückel limit. The second source of error is the effect of electrode polarization. Application of Eq. (15) to infer ζ tacitly assumes that streaming current is the only current in the system; however, a few hundred millivolts of polarization, as is typical on many electrodes in aqueous solutions, can be a significant contributor of error especially if the capillary resistance is not large (Fig. 4c). The polarization potential is equal to a logarithmic function of the current density plus the standard potential (*cf.* Butler-Vollmer equation [7]), resulting in the representation of the electrodes as diodes in the equivalent circuit. The hallmark of polarization is a nonlinear dependence of measured I_s on *P* applied, which can be subtle unless a large range of pressures is spanned during the measurement.

By measuring the streaming potential, some of the errors associated with streaming current measurements may be eliminated. In particular, streaming potential measurements draw so little current that electrode polarization problems are usually not significant if Ag/AgCl or platinized platinum electrodes are used. Furthermore, streaming potential measurements eliminate the dependence on cross-sectional area and the errors attendant with ill-specified geometry, such as microchannels with subtle etch depth variation. When streaming potential ($\Delta\phi$) is measured, the Smoluchowski equation is typically used to infer ζ:

$$\frac{\Delta\phi}{\Delta P} = \frac{\varepsilon\zeta}{\eta\sigma} \tag{16}$$

Streaming potential measurements must also occur in the thin EDL limit; if not, geometry-dependent corrections such as those in [25–27] need to be employed. At large ζ, the correction factor can be $>$10% even for Debye layers that are 1/50 the channel radius [26]. Also, the conductivity of the channel may be significantly affected by surface conduction [16], especially for small channels and low ionic strengths, and this must be corrected by measuring the apparent σ in the channel or capillary. Careful comparative studies employing both streaming potential and electroosmotic mobility show good agreement, as one might expect from Onsager reciprocity [4, 54]. Channels larger than 50 μm with ionic strengths $>$ 10 mM typically lead to negligible surface conductance, and in these cases the measurement is straightforward. The left-hand side of Eq. (16) is usually obtained as the slope of a streaming potential *vs.* pressure curve obtained while slowly varying the pressure and monitoring the voltage with a high impedance electrometer. Capacitance at the electrodes can lead to a long time constant for the system to reach equilibrium; measurements must be conducted by ramping the pressure up and down to confirm that no hysteresis is observed.

Combining multiple measurement techniques allows for error checking and, if performed very carefully, allows for investigation of more subtle aspects of double layer models. Werner *et al.* [55] note that it is possible to use these different methods (coupled with measurements of excess conduction), as complementary methods that allow one to assess possible differences in the location of inner and outer Helmholtz planes as well as the shear plane; Lyklema *et al.* [56] and Dukhin [9], for example, review data suggesting mobility of ions behind the OHP. Despite these claims, the details of the electric double layer structure are not well-known or agreed upon even for silica. Advanced apparatus for conducting these sorts of streaming measurements on flat surfaces [55] have the advantage of multi-measurement capability as well as a simple flow cell geometry. Measurements using multiple techniques are invaluable, since the errors with different techniques are often opposite in sign. For example, heating in electroosmotic measurements leads to erroneously high ζ results, while poor electrodes or neglecting to account for surface conductance in streaming potential measurements leads to erroneously low ζ results. Advanced measurement systems and multiple measurement techniques should lead to improved data as well as improved fundamental understanding of these phenomena.

4 Zeta potential on silica/silicon substrates

This section summarizes progress toward measuring and modeling the zeta potential in silica/silicon substrates. Since glass and silica capillaries have existed for dec-

ades, most of the work in silica has been performed in capillaries (in contrast, the data for polymeric substrates, discussed in the companion to this paper [1], is dominated by measurements in microfluidic chips). Discussion of functional dependences of ζ on solution parameters (pH, counterion concentration, counterion valency, counterion size, and temperature) is presented in the context of existing data. Silicon is also discussed briefly.

4.1 Glass and silica

Because of the extensive and long-standing use of glass capillaries for analytical techniques, the chemical properties of silica (and techniques for modifying same) are more well-known than those of any other microfluidic substrate material [57]. While the exact silicate types used for capillaries have typically differed from those used for microchips, zeta potential results do not vary significantly between silicate type. Capillaries have typically been manufactured from fused silica, with high-quality surface smoothness and low cation levels. Soda lime glass, though, has been the most common substrate used for microchip fabrication. While its cation levels are high, it is easily etched and relatively inexpensive. Both fused-silica and borofloat glasses have been used for etching planar microchips; however, they are more expensive, take longer to etch (or higher HF concentrations), and are often problematic due to poor surface finish or residual stress inhomogeneities. For the purposes of this section and discussion of ζ, different silica types will all be treated as equivalent. Table 1 summarizes several references that report measurement of ζ (or electroosmotic mobility*). From these, the effects of pH and counterion properties (concentration, valency, size) can be inferred.

4.1.1 Dependence of ζ on counterion concentration – empirical observations and comparisons with theory

Empirically, if the observed zeta potential is plotted against the negative logarithm of the molar counterion concentration (Fig. 5), a linear relationship is observed over a wide range of concentration [20, 37, 58]:

$$\zeta = a_0 + a_1 \cdot \mathrm{pC} \tag{17}$$

* As stated earlier, electroosmotic mobility or streaming potential/current can be used to infer ζ only *via* a double-layer model. The Smoluchowski equation typically used to infer ζ employs GCS double-layer theory and the Debye-Hückel approximation. While this technique leads to errors at high ζ, it has been used by all reports referenced here, so the data summarized here has in all cases been evaluated with this same technique in order to preserve consistency.

where a_0 and a_1 are functions of the pH, temperature, substrate material, and counterion type, and pC is defined as $-\log_{10} \sum_i n_i$, where concentrations n_i are summed over all counterionic species. For simplicity univalent electrolytes are assumed here, although Eqs. (8) and (9) retain the valency dependence. All counterions must be considered, including [H+] or [OH−], particularly at extreme pH and very low buffer concentration. If excluded, ζ *vs.* [K^+], for example, will flatten when [K^+] becomes less than [H^+]. For silica, Revil [20] gives a_1 at pH 7 for K^+ or Na^+ ions as $-kT/3e^-$ ln(10) ≈ -20 mV. a_0 is much more complicated, typically a function of many parameters, including site dissociation constants and surface silanol density, which are difficult to infer accurately from experiments and difficult to repeat. a_0 is nearly zero for sodium and potassium in Fig. 3, so for many separation buffers this equation can be simplified with generation of only small errors by setting $a_0 = 0$ in Eq. (17). In doing so, a very simple relation is obtained, valid only for cations that do not show specific adsorption:

$$\zeta \sim \mathrm{pC} \tag{18}$$

Equation (18) is consistent with the empirical observations (i) $\zeta \approx 0$ at pC = 0 and (ii) ζ scales linearly with pC, as shown in Fig. 3. This is also observed for sodium and potassium in polymer substrates [1]. For those situations in which this result is valid (small monovalent cations, $\zeta >$ 40 mV), this provides a powerful tool for normalizing complex sets of data from a wide variety of sources and evincing functional dependences. Some common additives prevent this relation from being used (many surfactants can exist in different micellar and bilayer orientations and do not follow such a simple relation [41, 59]). However, for simple buffers and small univalent cations the errors associated with this approximation are small down to $\zeta \approx 20$ mV, and the applicability of Eq. (18) (which is equivalent to Eq. 9) is quite wide-ranging.

The observation that $a_0 \approx 0$ for indifferent counterions allows Eq. (18) to show great usefulness as an engineering approximation; however, its applicability and theoretical justification must be distinguished from Eqs. (9) and (17) which follow directly from the thermodynamics of cation adsorption and the structure of the EDL in the high-ζ limit. In contrast, Eq. (18) is a convenient phenomenological approximation made possible by the serendipitous result that $a_0 \approx 0$ if units of M are used and indifferent counterions dominate the solution.

Evidence of the usefulness of Eq. (18) can be seen in Fig. 5, in which the ζ *vs.* pH data from two references [39, 40] are recast. The zeta potential is normalized by pC, and the normalization successfully collapses the data for each investigation onto a single curve. This suggests that it is

Table 1. Selected references with zeta potential or electroosmotic mobility measurements

Ref.	Technique[a)]	Counterion	Buffer ion	Comments
[20]	Various	Various	Various	Data in secondary references
[38]	EOM	$ACES^+/Na^+$	Phosphate, ACES	
[39]	SP	K^+	None	Extensive modeling presented
[40]	EPM	K^+	None	
[44]	EOM	Na^+	Various	Effects of CTMAB additive as function of concentration
[47]	EOM	K^+	None	
[51]	EOM	$Na^+/K^{+b)}$	Carbonate	Shows dependence of zeta potential in plastics on exposure to caged dye
[58]	EOM, SP	K^+	None	Compares SP to EOM and observes good match
[60]	EOM	Na^+	Unspecified	Shows hysteresis at pH 4–5
[62]	EOM	Na^+, Al^{3+}	None	Lower ζ than other references
[63]	EOM	Na^+, Li^+, K^+, Ba^{2+}, Ca^{2+}	Acetate	Shows minor difference between Na^+, Li^+, K^+ ; significant difference between Group I and Group II ions
[64]	ESA	K^+, Mg^{2+}	None	Shows reduction in ζ for Mg^{2+} as compared to K^+; shows need to correct for surface conductance
[65]	SP	K^+, La^{3+}	None	Shows effect of Group III ions on ζ
[96]	SP	Various	Various	
[97]	EOM	K^+	Various	Variation between pyrex and silica
[98]	EOM	$Na^+/K^{+b)}$	Phosphate	Effects of CTMAB additive
[99]	EOM	Na^+	Borate, citrate, phosphate	Most measurements in presence of SDS
[100]	SP, SC	Na^+	None	
[101]	SC	Na^+	None	Measured in porous bed – Kozeny-Carman modeling of flow
[102]	EOM	K^+	Phosphate	Dependence of ζ on organic solvents

a) Techniques: ESA, electrokinetic sonic amplitude; EOM, electroosmotic mobility; EPM, electrophoretic mobility; SP, streaming potential; SC, streaming current.

b) Cation unspecified, assumed Na^+ or K^+; ACES, *N*-(2-acetamido)-2-aminoethanesulfonate; CTMAB, cetyltrimethylammonium bromide

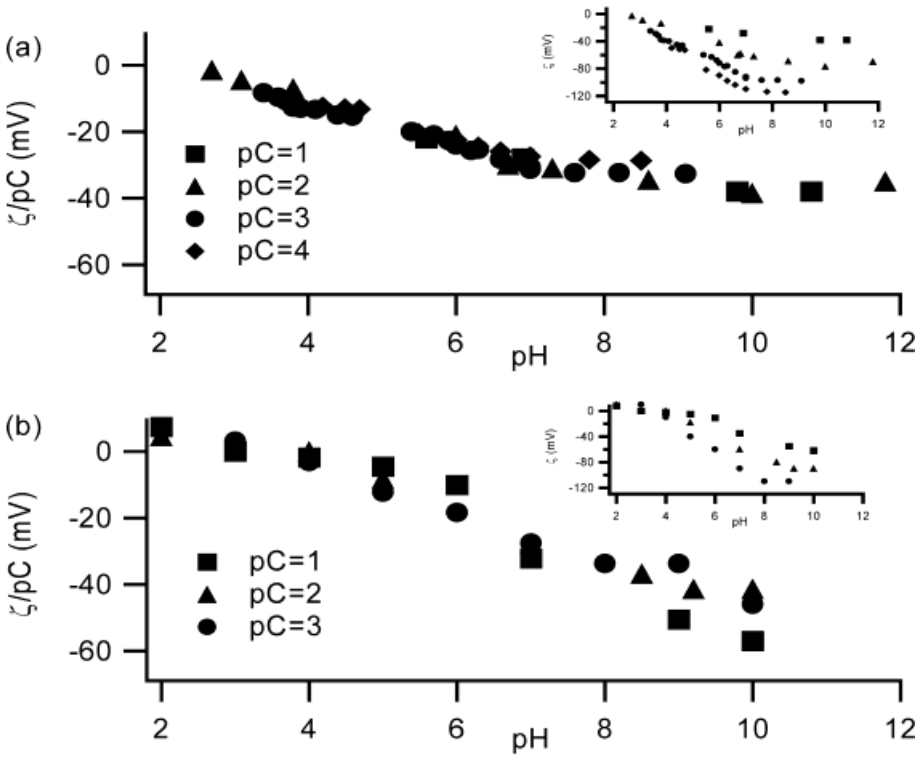

Figure 5. Zeta potential measured as a function of pH and counterion concentration. Top: data from Ref. [39]; bottom: data from Ref. [40]. In both cases, ζ is plotted normalized by pC as a function of pH. For both investigations, the ζ *vs.* pH relationship can be collapsed to a single curve over decades of counterion concentration change. Insets: plots of absolute ζ show variation if pC normalization is not employed.

possible to isolate concentration and pH effects from each other when analyzing ζ: pH affects protonation/deprotonation equilibria at the surface and affects charge density, while counterion concentration affects the degree to which the surface charge is shielded and the effective zeta potential observed by the flow. Because of the success of this normalization in simplifying interpretation of ζ data, ζ/pC will be plotted throughout this paper to facilitate comparison of data from varied sources.

4.1.2 Dependence of ζ on pH

For nonspecifically adsorbing counterions, the functional form of the variation of inferred zeta potential with pH is attributable to protonation or deprotonation of silanol sites and is, to first order, independent of the concentration. Figure 6 shows zeta potential measurements from five sources over a wide range of pH and approximately five decades of counterion concentration. In this figure, only results with small univalent cations (K^+, Na^+) are shown. The observed zeta potentials have been normalized by pC, so pH variations can be compared independent from concentration variation. Significant scatter is still observed between data sets from different investigators, even when data sets with similar counterion concentration are used. The body of data is inconclusive about

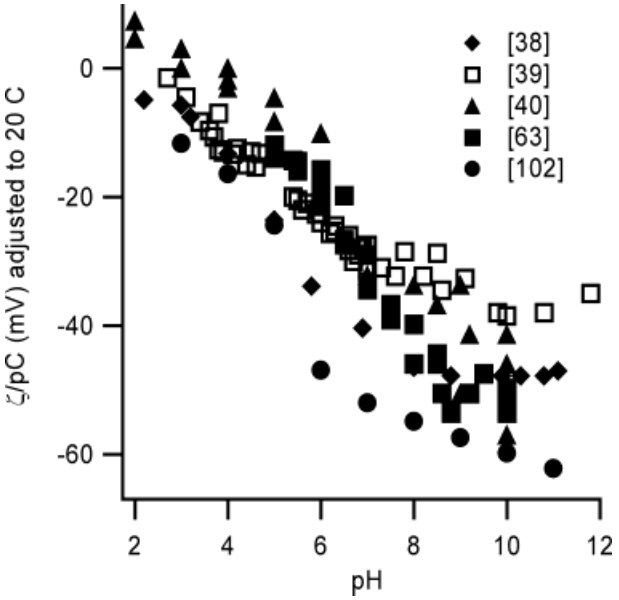

Figure 6. pH dependence of temperature-corrected (20°C), normalized zeta potential. Filled symbols: electroosmotic or electrophoretic mobility. Open symbols: streaming potential. For all data, the dominant cation is potassium or sodium. For clarity, results from only a few representative references are shown; additional data can be found in references listed in Table 1.

the detailed form of the pH dependence.* Many investigators find a linear variation with pH, while others show ζ plateaus at a pH near 8, at which all silanols are deprotonated. Certainly, if silanol deprotonation can be modeled with a single pK_a near 5, as has typically been reported, the zeta potential should plateau at high pH. It has been postulated that OH^- adsorption at high pH can explain the continued increase. Multiple investigators [18, 34, 60] have observed and modeled hysteresis in the zeta potential of silica in the 4–6 pH range, which equilibrates on long time scales (days). These experimental results have been theoretically explained in terms of the kinetics of a gel layer forming near the surface at low pH [18]. The scatter can be attributed to experimental error, subtle dependences on counterion type, and unattributed temperature changes. The rough functional form, though, is consistent among all measurements: zeta potential drops to zero near pH 2.7 and increases as pH is increased.

Significant effort has been devoted to developing a model for the silica/aqueous electrolyte interface that is quantitatively accurate. Most models for surface kinetics assume that the ionizable surface sites behave as weak polyprotic acids, while also allowing for the possibility of a metal ion exchange reaction with the counterions. The reaction constants are

$$K_1 = [H^+]_s[S^-]_s/[SH]_s \quad (19)$$

$$K_2 = [H^+]_s[SH]_s/[SH_2^+]_s \quad (20)$$

$$K_M = [H^+]_s[SM]_s/[M^+]_s[SH]_s \quad (21)$$

where S is an ionizable surface site (*e.g.*, SiO) and M^+ is a metal counterion. Boltzmann partitioning accounts for different activities at the surface (subscript *s*) as compared to bulk values (subscript *b*):

$$[H^+]_s = [H^+]_b\exp(-e\psi/kT), \quad (22)$$

$$[M^+]_s = [M^+]_b\exp(-e\psi/kT), \quad (23)$$

and an additional conservation equation can be written for ionizable sites

$$[SH_2^+]_s + [SH]_s + [S^-]_s = [S_o]_s \quad (24)$$

Various measurements show the surface site density $[S_o]_s$ of silica to range between 5×10^{14} [20] and 32×10^{14} sites/cm^2 [39]. This would appear to be enough equations to

* The wealth of data available for silica and the widely-varying results make clear that the results of a single investigator are insufficient for drawing conclusions. The data in Fig. 6 has been chosen to indicate the median results from a wealth of investigators; however, one can find a single reference to match nearly any ζ result. It is crucial when comparing observed ζ values to the literature that the preponderence of the observed values be used for comparison.

solve the system, but ambiguity remains regarding where ψ should be evaluated in the above equations for Boltzmann partitioning, and how to account for adsorbed ions, in addition to the constants K_1, K_2, and K_m not being known or agreed upon. As a result, the model presented by [39] has some other *ad hoc* assumptions about outer-layer capacitance; the model in [20] appears quite accurate but is limited to very low electrolyte concentrations. Many references [20, 32, 39, 61] report models of varying complexity; however, these models typically can be made to fit only narrow sets of data, and curve-fit parameters used to match one set of data invariably cannot be used to predict other data. When curve fits are used to infer double-layer or Stern layer properties, nonphysical results are typically obtained.

4.1.3 Dependence of ζ on temperature

The dependence of ζ on temperature stems from changes in the silanol equilibrium, adsorption equilibria, and diffuse double-layer thickness [20]. Within the region applicable to microchip separations, the zeta potential of silica increases approximately 1.75% per °C. Therefore, even minor temperature variations (*e.g.*, 5–10°C) are quite significant when zeta potential is calculated. Unfortunately, very little data exists on measurements of ζ as a function of temperature, so few comparisons can be made. Ref. [20] shows comparisons between experiment and modeling that show good agreement. Comparisons of zeta potentials cannot be made unless temperatures are well-specified – some attention to this has been paid but clearly many references show data affected by temperature fluctuations that have not been measured or corrected for. Electroosmotic mobility measurements have an inherent uncertainty because the temperature of the solution increases from the inlet to the outlet of a microchannel or capillary. To the extent possible, the data in Fig. 6 have been corrected for temperature variations using theoretical predictions [20] and correspond to the zeta potential at 20°C.

4.1.4 Dependence of ζ on counterion valency and size

Counterion valency and size and its effects on ζ are typically unimportant in separations, simply because the dominant counterion is in almost all cases potassium or sodium, and the observed differences between zeta potential observed in the presence of potassium *vs.* sodium are small compared to the scatter of the results. However, it is important to note the dependence of zeta on counterion valency and size so as to make possible predictions of zeta potential in cases where larger ions (*e.g.*, ions from biological buffers, *e.g.*, $HEPES^+$, $CAPS^+$ or $Tris^+$) or Group II/III ions (*e.g.*, Fe^{3+}, Ca^{2+}) dominate the counterion concentration.

Counterion valency and size influence the zeta potential by affecting surface adhesion equilibrium, by changing the exact location of the OHP, and by affecting the thickness of the diffuse double layer. The most easily modeled effect is the compression of the diffuse double-layer attendant with use of counterions of higher valency, as shown in Eq. (9). Comparisons of zeta potential on glass with Al^{3+}/Na^+[62], $Na^+/Li^+/K^+/Ba^{2+}/Ca^{2+}$ [63], and K^+/Mg^{2+} [64] all show reduction in zeta potential with higher valency ions as compared to lower valency ions. Similar reduction has been observed on both glass and poly(dimethyl siloxane) with La^{3+}/Na^+[65]. However, Eq. (9) is often not enough to describe valency effects, since many results show much more dramatic ζ reduction due to specific adsorption [63, 66, 67]. Reports vary as to whether variations with ion size among ions with common valency are well correlated [20, 63, 68, 69]; regardless, these variations are typically small as compared to experimental uncertainty and investigator-to-investigator scatter.

4.1.5 Zeta potential modification and control

Modification and control of zeta potential on silica surfaces is a heavily investigated subject; the majority of research effort has been on the suppression of zeta potential, and useful techniques include dynamic coatings, treatment with organosilanes, and deposition of polymer films [30, 41, 70–72]. Because of the extensive work in this area, appropriate treatment of this topic is beyond the scope of this paper.

4.2 Silicon

While silicon-based microfabrication techniques are very common, very few devices have been designed for microchip separation techniques. In all cases, the primary concern is achieving appropriate voltage standoff such that high electric field may be used for electroosmosis without experiencing large leakage current. Because the impact of silicon micromachining on electrokinetic microchip separations has been small, it will be treated only briefly here.

Because insulating layers must be used on silicon devices, the zeta potential performance on silicon devices is invariably dictated by the chemistry of insulative layers of SiO_2 or Si_3N_4. The charge sites on SiO_2 are invariably Si-OH, regardless of the silica type or deposition technique; hence thin SiO_2 layers perform much like bulk

silica. Furthermore, the dominant charge site on Si_3N_4 exposed to aqueous solutions is also Si-OH, with a minority (~1%) of Si-NH_2 sites [73]. Various investigators of silicon nitride powders or silicon nitride thin films [73, 74] have found roughly similar results, namely that the presence of Si-NH_2 sites on silicon nitride shifts the zeta potential *vs.* pH curve toward positive values. Ref. [73] has reported that HF etching removes Si-OH sites and increases the Si-NH_2 density, moving the pI from ~ 2.7 to ~ 3.9. Investigators have differed, though, on the long-term effect of storage and contact with aqueous solutions.

5 Implications for microchip separations

When applied to microchip separations, electroosmotic flow has the potential to lead to numerous improvements. In capillary zone electrophoresis, having a strong electroosmotic flow can ensure that both cationic and anionic analytes travel the same direction down the column, avoiding the need to instrument the system with two detectors (this is especially attractive for small portable systems). Unlike pressure-driven flow, the nearly uniform velocity profile of EOF across uniform channels of μm-scale dimensions introduces very little additional dispersion and thus minimal band broadening [27, 75]. Depending on the specific constraints of the system, EOF can also be exploited to minimize the analysis time by making elution occur precisely when the separation is complete. EOF can also be exploited in microchip analytical systems in many other ways. For example, EOF can be used to pump fluid for flow-injection analysis [76], or used in porous matrices to generate high pressure for applications such as HPLC [77, 78]. Much work has been performed recently [79] to explore these pumps for a myriad of applications in microchip devices as well as macroscale pumping applications.

However, despite these benefits, the drawbacks of EOF in many CE applications can be significant and can greatly outweigh its advantages. One of these drawbacks is that, if there are any variations in the conductivity (*e.g.*, ionic strength), zeta potential (*e.g.*, pH, ionic strength, substrate material or coating), viscosity, or permittivity of the fluid, significant pressure-driven flow (PDF) can occur [80] (even if the imposed pressure difference across the capillary is zero), and PDF can cause very rapid dispersion (band broadening). Such axial variations can occur intentionally (*e.g.*, sample stacking [81–83]) or unintentionally (*e.g.*, due to protein adsorption [84] or due to hydrolytic evolution of the electrode reservoirs [53]). Another drawback is that composite microchannels constructed from two or more materials will lead to extreme dispersion unless the zeta potentials are perfectly matched. This is of particular pertinence to polymer systems, which routinely use two different materials for microchip and cover. Separations in poly(dimethyl siloxane) (PMDS) bonded to glass, for example [85] have been shown to be significantly inferior as compared to those in silica.

An analytical solution for axial variation effects, for the special case of periodic variations in ζ along the axial direction has been presented [48], in the form of an asymptotic series solution for the velocity field for any arbitrary function ζ(*x*). Figure 7 shows streamlines for sinusoidal variations; these streamlines approximate (to first order) those that might occur, for example, with UV-polymerized coating patterned periodically along a microchannel. As the magnitude of the variation in ζ grows compared with its mean value, the streamlines evolve to become recirculatory; the adverse effect such streamlines could have on separation efficiency are obvious. On the other hand, patterning ζ in such a way could be quite effective if mixing is desired. A very similar idea was recently explored [86] by computing patterns for in-channel binary fluid "mixers" comprised of solvophobic/solvophilic patches.

Significant recent work in the last decade specifically addresses the effects of axial ζ variation on CE. Both experimental data and modeling have been presented,

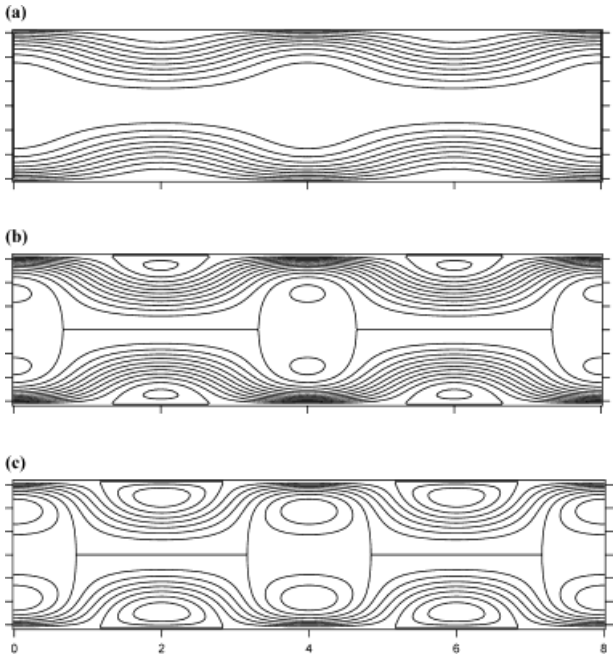

Figure 7. Plots of the flow streamlines produced by sinusoidal variations in ζ in the direction of the capillary axis, produced using equations presented in [48]. (a) $\zeta = \zeta_o (1+\sin 2\pi x)$; (b) $\zeta = \zeta_o(1+2\sin\pi x)$ (c) $\zeta = \zeta_o (1+4\sin 2\pi x)$.

with attention to protein adsorption on silica [87]. In general, the hydrodynamics have been considered in the limit of slowly varying $\zeta(x)$. Numerical investigation of the flow and analyte transport for various coated/uncoated sections in series has been presented [88]. A simplified analytical model for the hydrodynamics and dispersion assuming largely 1-D flow comprised of superposed pure PDF and pure EOF profiles has been shown to agree well with experimental results achieved using caged-dye imaging [89]. Asymptotic treatment of the hydrodynamics and transport in the limit of slow axial ζ variations (the "lubrication theory limit"), including analyte adsorption kinetics has been successful in predicting experimental results quantitatively [90–92].

The various sources of axial dispersion can be generalized to show that variations in the quantity $\varepsilon\zeta/\eta\sigma$, also known as the Smoluchowski parameter, create nonuniform EOF and therefore result in PDF. A simple 1-D flow model in the "lubrication-theory limit", wherein the flow is assumed to be entirely in the axial direction can be used to show this. Lubrication theory is an accurate approximation if variations (in the axial direction) of these quantities occur slowly (*i.e.*, over distances $>$ 10 diameters), or in regions of the capillary that are at least 10 diameters away from any abrupt changes. In this limit, the flow is a linear superposition of an EOF component u_{eo} (approximately uniform axially) and a PDF component u_p (parabolic or similar "peaked" profile, depending on channel cross-section geometry). For a constant-area channel, mass continuity requires that

$$\bar{u} = \bar{u}_{eo} + \bar{u}_p = \text{const} \tag{25}$$

where $\bar{u}$, $\bar{u}_{eo}$, and $\bar{u}_p$ are the mean values across the channel cross-section. Since $\bar{u}$ is not a function of x (the distance along the channel), if $\bar{u}_{eo}$ varies, $\bar{u}_p$ is created to make up the difference. Substitution of the equation for current continuity into the equation for EOF (Eq. 5) leads to

$$u_{eo} = \frac{I}{A}\left(\frac{\varepsilon\zeta}{\sigma_{app}\eta}\right) \tag{26}$$

where σ_{app} is the apparent local fluid conductivity (including surface conduction) and I is the total current in the capillary, which must be constant. Thus u_{eo} varies, and generates PDF, if the quantity $\varepsilon\zeta/\eta\sigma$ varies. The PDF leads to Taylor-Aris dispersion (band broadening) [93–95], which is highly undesirable for efficient separation.

Variations in the Smoluchowski parameter can easily arise in microchip separation systems, due to the flexibility that the designer has to intersect channels arbitrarily, and thereby fill different sections of channels with different electrolyte solutions; this can lead to changes in all four properties in the Smoluchowski parameter. It is also possible to coat the channel walls selectively using UV- or hydrodynamically patterned surface coatings [72]. Finally, different materials and fabrication processes can lead to varying uniformity of zeta potential; for example some recent work [52] has indicated that poly(methyl methacrylate) has a particularly nonuniform zeta potential as compared to poly(dimethyl siloxane) and silica. Cross-sectional area changes in the channel do not normally generate PDF because the flow continuity and current continuity equations are both affected in the same way. However, PDF can be generated if there is a dramatic increase in the apparent conductivity due to surface conduction or nonuniform Joule heating.

6 Conclusions

The preceding sections have presented theory, experimental techniques, and the reported data pertaining to the zeta potential of microfluidic substrate materials with specific attention to glass and silica, and commented on the effects of zeta potential and its variations on separations. It has been shown that for most situations relevant to microchip separations, the zeta potential on silica substrates is proportional to the logarithm of the molar counterion concentration; hence normalization of zeta potential can be used to collapse complex data sets. Ionic strength, buffer concentration, and counterion concentration have all been used to describe the solutions used in experiments but they apply to different aspects of ζ. Ionic strength is important for species that ion exchange with the wall, particularly divalent cations. Buffer type and concentration typically do not affect results other than through the counterion concentration which is invariably related. Counterion concentration affects charge shielding in the double layer. Due to the strong dependence of ζ on temperature, significant scatter in the observed data can also be explained by temperature variations and eliminated with simple temperature corrections.

Several experimental techniques have been used to measure ζ in capillaries, films, and microfluidic substrates. ζ values measured using electroosmotic and electrophoretic mobility tend to be larger than those for streaming potential and current techniques. This is most likely since the most common errors for these techniques lead to errors in opposite directions – electroosmotic/electrophoretic mobility measurements tend to overestimate ζ in the presence of finite Joule heating, while streaming potential techniques underestimate ζ if electrodes are not carefully manufactured and monitored or if surface conductance is ignored.

These observations point to a number of recommendations for how ζ may be best measured and reported. First, it is crucial to record and control temperature. Even a 5°C variation in temperature will lead to ζ errors larger than the precision claimed by most investigators. Second, it is crucial to record and report the counterion and its concentration. Measurements of ζ as a function of pH are best measured at constant counterion concentration, which is different from the more common approaches of keeping buffer concentration or ionic strength constant. Third, ζ *vs.* pH data is best presented in normalized fashion (*e.g.*, ζ/pC), to facilitate comparison between investigators. Fourth, measurements of ζ are most effective when measured at several pH values and (when possible) compared with multiple previous reports. Fifth, it is crucial to precisely describe the solutions used when reporting zeta potential measurements, so that the effects of counterion shielding, ion-exchange, and pH are well-specified. Finally, zeta potential measurements are most effective when performed using two techniques, *e.g.*, streaming potential and electroosmotic mobility.

Received October 17, 2003

7 References

[1] Kirby, B. J., Hasselbrink Jr., E. F., *Electrophoresis* 2004, *25*, 203–213.

[2] Hunter, R. J., *Foundations of Colloid Science*, Vol. 2, Clarendon Press,Oxford 1989.

[3] Lyklema, J. H., *Fundamentals of Interface and Colloid Science*, Academic Press, London 1991.

[4] Kralchevsky, P. A., Danov, K. D., Denkov, N. D., in: Birdi, K. S. (Ed.), *Handbook of Surface and Colloid Chemistry*, CRC Press, Boca Raton, FL 2003, p. 137.

[5] Gileadi, E., Kirowa-Eisner, E., Penciner, J., *Interfacial Electrochemistry: An Experimental Approach*, Addison-Wesley, Reading, MA 1975.

[6] Overbeek, J. T. G., *Colloid Science, Vol. 1*, Elsevier, Amsterdam 1952.

[7] Bard, A. J., Faulkner, L. R., *Electrochemical Methods: Fundamentals and Applications*, Wiley, New York 2001.

[8] Vanderput, A. G., Bijsterbosch, B. H., *J. Coll. Int. Sci.* 1980, *75*, 512–524.

[9] Dukhin, A. S., Vandeven, T. G. M., *J. Coll. Int. Sci.* 1994, *165*, 9–18.

[10] Shubin, V. E., Hunter, R. J., Obrien, R. W., *J. Coll. Int. Sci.* 1993, *159*, 174–183.

[11] Midmore, B. R., Hunter, R. J., *J. Coll. Int. Sci.* 1988, *122*, 521–529.

[12] Zukoski, C. F., Saville, D. A., *J. Coll. Int. Sci.* 1986, *114*, 32–44.

[13] Zukoski, C. F., Saville, D. A., *J. Coll. Int. Sci.* 1986, *114*, 45–53.

[14] Zukoski, C. F., Saville, D. A., *J. Coll. Int. Sci.* 1985, *107*, 322–333.

[15] Lyklema, J., Rovillard, S., De Coninck, J., *Langmuir* 1998, *14*, 5659–5663.

[16] Lyklema, J., Minor, M., *Coll. Surf. A* 1998, *140*, 33–41.

[17] Hunter, R. J., *Adv. Coll. Int. Sci.* 2003, *100*, 153–167.

[18] Huang, T. L., *Chromatographia* 1993, *35*, 395–398.

[19] Yates, D. E., Levine, S., Healy, T. W., *J. Chem. Soc. Farad. Trans.* 1974, *70*, 1807–1818.

[20] Revil, A., Pezard, P. A., Glover, P. W. J., *J. Geophys. Res.* 1999, *104*, 20021–20031.

[21] Freund, J. B., *J. Chem. Phys.* 2002, *116*, 2194–2200.

[22] Freund, J. B., *Phys. Fluids* 2003, *15*, L33–L36.

[23] Zhang, X. Y., Zhu, Y. X., Granick, S., *Science* 2002, *295*, 663–666.

[24] Reiter, G., Demirel, A. L., Granick, S., *Science* 1994, *263*, 1741–1744.

[25] Burgreen, D., Nakache, F. R., *J. Phys. Chem.* 1964, *68*, 1084–1094.

[26] Rice, C. L., Whitehead, R., *J. Phys. Chem.* 1965, *69*, 4017–4024.

[27] Griffiths, S. K., Nilson, R. H., *Anal. Chem.* 2000, *72*, 4767–4777.

[28] Griffiths, S. K., Nilson, R. H., *Anal. Chem.* 1999, *71*, 5522–5529.

[29] Hückel, E., *Phys. Z.* 1924, *25*, 204–210.

[30] Corradini, D., *J. Chromatogr. B* 1999, *699*, 221–256.

[31] Salomon, K., Burgi, D. S., Helmer, J. C., *J. Chromatogr.* 1991, *549*, 375–385.

[32] Salomon, K., Burgi, D. S., Helmer, J. C., *J. Chromatogr.* 1991, *559*, 69–80.

[33] Atamna, I. Z., Issaq, H. J., Muschik, G. M., Janini, G. M., *J. Chromatogr.* 1991, *588*, 315–320.

[34] Reid, R. H. P., *J. Chromatogr. A* 1994, *669*, 155–161.

[35] Tsuda, T., Nomura, K., Nakagawa, G., *J. Chromatogr.* 1982, *248*, 241–247.

[36] Issaq, H. J., Atamna, I. Z., Muschik, G. M., Janini, G. M., *Chromatographia* 1991, *32*, 155–161.

[37] Hunter, R. J., Wright, H. J. L., *J. Coll. Int. Sci.* 1971, *37*, 564–580.

[38] Caslavska, J., Thormann, W., *J. Microcol. Sep.* 2001, *13*, 69–83.

[39] Scales, P. J., Grieser, F., Healy, T. W., *Langmuir* 1992, *8*, 965–974.

[40] Kosmulski, M., Matijevic, E., *Langmuir* 1992, *8*, 1060–1064.

[41] Melanson, J. E., Baryla, N. E., Lucy, C. A., *TrAC* 2001, *20*, 365–374.

[42] Somasundaran, P., Healy, T. W., Fuerstenau, D. W., *J. Phys. Chem.* 1964, *68*, 3562–3566.

[43] Fuerstenau, D. W., *J. Phys. Chem.* 1956, *60*, 981–985.

[44] Altria, K. D., Simpson, C. F., *Chromatographia* 1987, *24*, 527–531.

[45] Bikerman, J. J., *Trans. Farad. Soc.* 1940, *36*, 154–159.

[46] Hidalgo-Alvarez, R., *Adv. Coll. Int. Sci.* 1991, *34*, 217–341.

[47] Arulanandam, S., Li, D., *J. Coll. Int. Sci.* 2000, *225*, 421–428.

[48] Anderson, J. L., Idol, W. K., *Chem. Eng. Commun.* 1985, *38*, 93–106.

[49] Mosier, B. P., Molho, J. I., Santiago, J. G., *Exp. Fluids* 2002, *33*, 545–554.

[50] Paul, P. H., Garguilo, M. G., Rakestraw, D. J., *Anal. Chem.* 1998, *70*, 2459–2467.

[51] Ross, D., Locascio, L. E., *Anal. Chem.* 2003, *1*, 1218–1220.

[52] Ross, D., Johnson, T. J., Locascio, L. E., *Anal. Chem.* 2001, *1*, 2509–2515.

[53] Bello, M. S., *J. Chromatogr. A* 1996, *744*, 81–91.

[54] Morrison, F. A., Osterle, J. F., *Energy Conversion* 1969, *9*, 7–12.

[55] Werner, C., Korber, H., Zimmermann, R., Dukhin, S., Jacobasch, H. J., *J. Coll. Int. Sci.* 1998, *208*, 329–346.

[56] Lyklema, J., *J. Phys. Cond. Matt.* 2001, *13*, 5027–5034.

[57] Iler, R. K., *The Chemistry of Silica*, Wiley, New York 1979.

[58] Johnson, P. R., *J. Coll. Int. Sci.* 1999, *209*, 264–267.

[59] Lucy, C. A., Underhill, R. S., *Anal. Chem.* 1996, *68*, 300–305.

[60] Lambert, W. J., Middleton, D. L., *Anal. Chem.* 1990, *62*, 1585–1587.

[61] Birli, C., Piaggio, M. V., Deiber, J. A., *Electrophoresis* 2003, *24*, 1587–1595.

[62] Gu, Y., Li, D., *J. Coll. Int. Sci.* 2000, *226*, 328–339.

[63] Dickens, J. E., Gorse, J., Everhart, J. A., Ryan, M., *J. Chromatogr. B* 1994, *657*, 401–407.

[64] Löbbus, M., Sonnfeld, J., van Leeuwen, H. P., Vogelsberger, W., Lyklema, J., *J. Coll. Int. Sci.* 2000, *229*, 174–183.

[65] Sze, A., Erickson, D., Ren, L. Q., Li, D. Q., *J. Coll. Int. Sci.* 2003, *15*, 402–410.

[66] Chen, S., Pietrzyk, D. J., *Anal. Chem.* 1993, *65*, 2770–2775.

[67] Pietrzyk, D. J., Chen, S., Chanthawat, B., *J. Chromatogr. A* 1997, *775*, 327–338.

[68] Oefner, P. J., Bonn, G. K., Huber, C. G., Nathakarnkitkool, S., *J. Chromatogr.* 1992, *625*, 331–340.

[69] Atamna, I. Z., Metral, C. J., Muschik, G. M., Issaq, H. J., *J. Liq. Chromatogr.* 1990, *13*, 2517–2527.

[70] Millot, M. C., Vidal-Madjar, C., *Adv. Chromatogr.* 2000, *40*, 427–466.

[71] Ito, Y., *Biomaterials* 1999, *20*, 23–24.

[72] Kirby, B. J., Wheeler, A. R., Zare, R. N., Fruetel, J. A., Shepodd, T. J., *Lab Chip* 2003, *3*, 5–10.

[73] Bousse, L., Mastarshed, S., *J. Elect. Chem.* 1991, *201*, 268–274.

[74] Jaffrezic-Renault, N., De, A., Clechet, P., Maaref, A., *Coll. Surf.* 1989, *36*, 59–68.

[75] Gaš, B., Stedry, M., Kenndler, E., *J. Chromatogr. A* 1995, *709*, 63–68.

[76] Dasgupta, P. K., Liu, S., *Anal. Chem.* 1994, *66*, 1792–1798.

[77] Paul, P. H., Arnold, D. W., Rakestraw, D. J, in: Banff, B. C. (Ed.), *MicroTAS '98*, Kluwer Academic, Enschede 1998, p. 149.

[78] Paul, P. H., Arnold, D. W., Neyer, D. W., Smith, K. B., in: *MicroTAS 2000*, Kluwer Academic, Enschede 2000, p. 583.

[79] Reichmuth, D. S., Kirby, B. J., *J. Chromatogr. A* 2003, *1013*, 93–101.

[80] Roberts, G. O., Rhodes, P. H., Snyder, R. S., *J. Chromatogr.* 1989, *480*, 35–67.

[81] Chien, R. L., *Anal. Chem.* 1991, *63*, 2866–2869.

[82] Burgi, D. S., Chien, R. L., *Anal. Chem.* 1991, *63*, 2042–2047.

[83] Vinther, A., Soeberg, H., *J. Chromatogr.* 1991, *559*, 3–26.

[84] Towns, J. K., Regnier, F. E., *Anal. Chem.* 1991, *63*, 1126–1132.

[85] Lacher, N. A., de Rooij, N. F., Verpoorte, E., Lunte, S. M., *J. Chromatogr. A* 2003, *1004*, 225–235.

[86] Kuksenok, O., Yeomans, J. M., Balazs, A. C., *Langmuir* 2001, *17*, 7186–7190.

[87] Towns, J. K., Regnier, F. E., *Anal. Chem.* 1992, *64*, 2473–2478.

[88] Potocek, B., Gaš, B., Kenndler, E., Stedry, M., *J. Chromatogr. A* 1995, *709*, 51–62.

[89] Herr, A. E., Molho, J. I., Santiago, J. G., Mungal, M. G., Kenny, T. W., Garguilo, M. G., *Anal. Chem.* 2000, *1*, 1053–1057.

[90] Ghosal, S., *Anal. Chem.* 2002, *74*, 4198–4203.

[91] Ghosal, S., *J. Fluid Mech.* 2002, *459*, 103–128.

[92] Ghosal, S., *Anal. Chem.* 2002, *74*, 771–775.

[93] Wooding, R. A., *J. Fluid Mech.* 1960, *7*, 501–515.

[94] Taylor, G., *Proc. Royal Soc. Lond.* 1953, *219*, 186–203.

[95] Aris, R., *Proc. Royal Soc. Lond.* 1956, *235*, 67–77.

[96] Reijenga, J. C., Aben, G. V. A., Verheggen, T. P. E. M., Everaerts, F. M., *J. Chromatogr.* 1983, *260*, 241–254.

[97] Lukacs, K. D., Jorgenson, J. W., *J. High Resolut. Chromatogr.* 1985, *8*, 407–411.

[98] Janini, G. M., Chan, K. C., Barnes, J. A., Muschik, G. M., Issaq, H. J., *J. Chromatogr. A* 1993, *653*, 321–327.

[99] Xu, W., Uchiyama, K., Shimosaka, T., Hobo, T., *J. Chromatogr. A* 2001, *907*, 279–289.

[100] Voigt, A., Wolf, H., Lauckner, H., Neumann, G., Becker, R., Richter, L., *Biomaterials* 1983, *4*, 299–304.

[101] Rodier, E., Dodds, J., *Part. Part. Sys. Char.* 1995, *12*, 198–203.

[102] Schwer, C., Kenndler, E., *Anal. Chem.* 1991, *63*, 1801–1807.

[103] Gaudin, A. M., Fursteneau, D. W., *Trans. ASME* 1955, *202*, 66–72.